Generalized grid-forming droop control for three-wire connection

Prajwal Bhagwat and Dominic Groß

Abstract—**In this work, we investigate generalized grid-forming (GFM) control for three-phase/three-wire dc/ac voltage source converters (VSCs) under unbalanced system conditions and faults. To fully leverage the degrees of freedom of VSCs with three-wire connection, we propose a generalized two-phase GFM control that combines individual GFM controls for two controllable phases with a phase balancing feedback and suitable three-wire implementations of the current saturation algorithm (CSA) and threshold virtual impedance (TVI). The proposed control enables current limiting for all three phases during unbalanced faults, reduces to positive sequence GFM droop control in balanced systems and is suitable to work both in stand-alone and grid-connected systems. High-fidelity simulations are used to illustrate the properties of the control.**

I. Introduction

Inverter-based resources (IBRs) are being deployed on the power grid at an ever-increasing rate. Stand-alone IBRs (e.g., uninterruptible power supplies) are already widely used for homes, businesses, and data centers, and their penetration is expected to see further growth [1]. Meanwhile, increased renewable generation motivates widespread adoption of inverter controls that explicitly address practical issues such as unbalanced operating conditions and unbalanced fault ride through for both four-wire and three-wire systems. Primarily these controls can be divided into grid-forming (GFM) and grid-following control [2].

While grid-following (GFL) converters can provide some grid support functions [2], [3], they require other devices to form a stable ac voltage waveform that GFL converters can lock on to. The GFM converters however can impose a well-defined and stable ac voltage waveform at their point of connection [4]. GFM converters are advantageous during contingencies due to their faster dynamics. However, limiting current to protect their semiconductor switches is a major challenge, especially during unbalanced faults.

Works that consider GFM control of grid-connected IBRs under unbalanced faults (e.g., [5]) typically leverage symmetrical components, e.g., implementing separate GFM controls for positive and negative sequence. This approach is motivated by standard power system analysis methods for unbalanced faults using symmetrical components. However, the relationship between the converter phase currents and symmetrical components is highly nonlinear [5] resulting in challenging control design and analysis problems. In contrast, [6] proposed to limit phase currents directly for voltage source converters (VSCs) with four-wire connection (e.g., grounded dc midpoint, wye-ground connected filter capacitors). While this approach allows GFM converters to maximize their degrees of freedom, the results in [6] do not directly apply to VSCs with three-wire connection commonly used for utility-scale IBRs.

In a three-wire connection, the LC output filter capacitors of VSC can be arranged in a wye configuration (see, e.g., [7]–[9]), or a delta configuration (see, e.g., [10]). Typically, in the literature, stand-alone uninterruptible power supply (UPS) systems with wye-connected output filter capacitors are considered and the focus is on supplying non-linear loads efficiently. A dual-loop Lyapunov-based control scheme is proposed in [9] which focuses on large signal stability of three-phase stand-alone inverters with improved robustness to nonlinear loads. Similarly, the work in [8] applies dual-loop control and utilizes double synchronous reference frame control. The work in [7] takes a different approach by applying multi-objective model predictive control (MPC) which finds analytical solution of a cost function tailored to the objective of generating optimal reference voltages for stand-alone VSCs. Despite being computationally expensive, none of these methods take fault current limiting into consideration in the design of their controls. A basic control scheme for delta-connected filter capacitors that does not account for the restrictions of three-wire connections is presented in [10].

In contrast, the GFM control for three-phase/three-wire grid-connected two-level dc/ac VSCs proposed in this work develops a control that leverages the capabilities of VSCs to control two line-to-line voltages to regulate all the output voltages and line currents such that, during unbalanced loading or faults, (i) the line current does not exceed the semiconductor current limits, and (ii) the line-to-line voltages are balanced whenever possible. To achieve this, we implement single-phase GFM control for two controllable phases and combine it with a balancing feedback that controls the trade-off between three-phase voltage unbalance and unbalance of the converter power injection between phases. We leverage the two-wattmeter method (see [11]) to develop a two-phase GFM droop control. The GFM voltage references are then tracked by an inner voltage and current control that separately control the two controllable VSC phases. The currents of two phases are controlled to implicitly control the third phase current to limit all three of them during unbalanced faults. This control architecture fully leverages the remaining degrees of freedom of three-wire connected VSCs (see [12] for details on current limits of three-wire connected VSC). To limit

This material is based upon work supported by the U.S. Department of Energy's Office of Energy Efficiency and Renewable Energy (EERE) under the Solar Energy Technologies Office Award Number 38637. The views expressed herein do not necessarily represent the views of the U.S. Department of Energy or the United States Government. D. Groß and P. Bhagwat are with the Department of Electrical and Computer Engineering at the University of Wisconsin-Madison, USA; e-mail: {dominic.gross,pbhagwat2}@wisc.edu.

979-8-3315-8138-1

line currents, both the reference current saturation algorithm and threshold virtual impedance [13] are adapted to three-wire connections. As a result, the proposed GFM control can maintain independent control of two line-to-line terminal voltages of VSC under unbalanced conditions while keeping the phase currents within their limits in both stand-alone and grid-connected operation. Finally, we demonstrate these features using electromagnetic transient (EMT) simulations.

II. Control objectives

The control proposed in this paper is inspired by the generalized three-phase GFM control of two-level dc/ac converter with wye connected filter and dc midpoint grounding described in [6]. In contrast, this work considers control of a grid-connected two-level three-phase dc/ac VSC with three-wire connection and floating dc bus. Consequently, in contrast to the setting in [6], the VSC cannot independently control its three line currents and its three terminal line-to-neutral voltages. The key control objectives for the GFM control proposed in this work are to (i) impose a well-defined and stable ac line-to-line voltage waveform at its terminal, (ii) asymptotically track controllable steady-state dispatch signal under nominal system conditions, (iii) autonomously respond to contingencies as well as variations in load and generation to stabilize the system, and (iv) operate within the VSC current limits on all three phases. Additionally, the proposed control reduces to the well-known (positive-sequence) GFM droop control under balanced conditions, and allows trading off three-phase voltage unbalance with current/power unbalances between phases during unbalanced loading through tuning of phase-balancing feedback gains.

III. Review of generalized three-phase GFM droop control for four-wire connection

To make this work self-contained, we briefly review the generalized three-phase droop control [6] for four-wire connection (e.g., using a two-level VSC with dc midpoint connected to a neutral wire or neutral of a wye transformer). In [6], since the ac filter capacitor neutrals and dc midpoint are grounded, all three-phase voltages and currents can be controlled to maximize all degrees of freedom of two-level VSCs. In particular, the GFM controller generates a frequency $\omega_p^{\text{gfm}} \in \mathbb{R}$ and angle $\theta_p^{\text{gfm}} \in [0, 2\pi)$ for each phase $p \in \mathcal{P}$ where $\mathcal{P} := \{a, b, c\}$. The frequency and angle references are also used to estimate phasors of the filter currents $i_p \in \mathbb{R}$ and filter capacitor voltages $v_p \in \mathbb{R}$ for each phase $p \in \mathcal{P}$. To this end, for all $p \in \mathcal{P}$ and any sinusoidal ac signal $x(t)$, we estimate the quadrature component $x_p^{\perp}(t) \in \mathbb{R}$ of $x_p(t) \in \mathbb{R}$ as

$$x_p^{\perp}(t) := x_p\big(t - \tfrac{1}{4}\tfrac{1}{\omega_p^{\text{gfm}}(t)}\big). \tag{1}$$

The quarter-cycle time shift in (1) is commonly referred to as Hilbert transform and can be interpreted as representing $\alpha\beta$ components of an ac signal (i.e., $(x_{p,\alpha}, x_{p,\beta}) = (x_p, x_p^{\perp})$). Let $\mathcal{R}(\cdot)$ denote the 2D rotation by the angle $\theta \in [0, 2\pi)$, i.e.,

$$\mathcal{R}(\theta) := \begin{bmatrix} \cos(\theta) & -\sin(\theta) \\ \sin(\theta) & \cos(\theta) \end{bmatrix}. \tag{2}$$

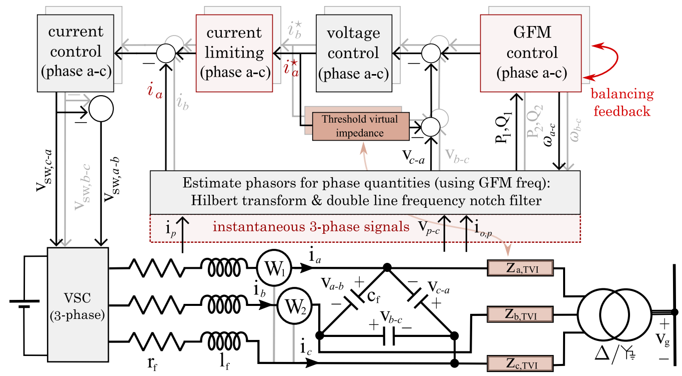

Fig. 1. Generalized two-phase GFM control for three-wire systems and inner control for tracking a voltage reference provided by the outer two-phase GFM control (4) with phase balancing feedback.

Then, any ac signal $x_p(t)$ can be represented in a dq frame with reference angle $\theta_p^{\text{gfm}}(t)$ as $x_{p,dq}(t) := \mathcal{R}(\theta_p^{\text{gfm}}(t))[x_p(t), x_p^{\perp}(t)]^{\mathsf{T}}$.

Finally, for all phases $p \in \mathcal{P}$, the average active power P_p and reactive power Q_p over one cycle can be computed as,

$$P_p(t) = \tfrac{1}{2}\left(v_p(t)i_p(t) + v_p^{\perp}(t)i_p^{\perp}(t)\right), \tag{3a}$$
$$Q_p(t) = \tfrac{1}{2}\left(v_p^{\perp}(t)i_p(t) - v_p(t)i_p^{\perp}(t)\right). \tag{3b}$$

IV. Generalized two-phase GFM droop control for three-wire connection

A. *Generalized two-phase GFM control*

In a grid-connected two-level dc/ac converter with three-wire connection (see Fig. 1) zero-sequence current cannot flow. Therefore, one phase becomes dependent on the other two. As a result, only two line-to-line voltages can be controlled. A VSC with delta-connected filter, filter resistance $r_f \in \mathbb{R}_{>0}$, filter inductance $l_f \in \mathbb{R}_{>0}$, and filter capacitance $c_f \in \mathbb{R}_{>0}$ for all three phases is shown in Fig. 1. The generalized two-phase control architecture actively controls phases a and b, while phase c is implicitly controlled. For the purpose of control design, phase c is treated as a virtual ground (see Ch. 10 of [11]), allowing voltage readings for phases a and b relative to it. In this configuration, the converter active and reactive power output, which serves as an input to the two-phase GFM controls, can be computed using the two-wattmeter method [11, Ch. 10]. Using (1), we define $P_1(t), Q_1(t)$ using the line-to-line filter voltage $v_{a-c}(t)$ and filter current $i_a(t)$, and $P_2(t), Q_2(t)$ using the line-to-line filter voltage $v_{b-c}(t)$ and filter current $i_b(t)$ as shown in Fig. 1. This results in

$$P_1(t) := v_{a-c}(t)i_a(t) + v_{a-c}^{\perp}(t)i_a^{\perp}(t), \tag{4a}$$
$$Q_1(t) := v_{a-c}^{\perp}(t)i_a(t) - v_{a-c}(t)i_a^{\perp}(t), \tag{4b}$$
$$P_2(t) := v_{b-c}(t)i_b(t) + v_{b-c}^{\perp}(t)i_b^{\perp}(t), \tag{4c}$$
$$Q_2(t) := v_{b-c}^{\perp}(t)i_b(t) - v_{b-c}(t)i_b^{\perp}(t). \tag{4d}$$

In (4), $v_{p-c} := v_p - v_c$ where $p \in \{a, b\}$ and (4) models the power measured by the wattmeters W_1 and W_2 in Fig. 1. Similar to [6], we re-write the droop equations for generalized GFM droop control of line-to-line voltages using the magnitude V_{p-c}^{gfm} and frequency ω_{p-c} of line-to-line voltages.

979-8-3315-8138-1

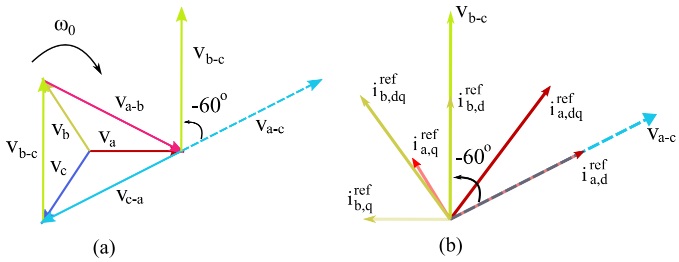

Fig. 2. Line-to-line and line-to-neutral voltage phasors (a) and current phasors with respect to line-to-line voltage phasors in a dq frame with angles $\theta_{a-c}^{\text{gfm}}$ and $\theta_{b-c}^{\text{gfm}}$ (b).

Considering $(\theta_{a-c}^{\text{bal}}, \theta_{b-c}^{\text{bal}}) := (0, -\frac{\pi}{3})$ (see Fig. 2 (a)) and voltage setpoints $V_{p-c}^{\star}$, the GFM voltage angle and magnitude references $\theta_{p-c}^{\text{gfm}} = \delta_{p-c}^{\text{gfm}} + \theta_{p-c}^{\text{bal}}$, where $\frac{\mathrm{d}}{\mathrm{d}t}\theta_{p-c}^{\text{gfm}} := \omega_{p-c}$, and $V_{p-c}^{\text{gfm}} = V_{\delta,p-c}^{\text{gfm}} + V_{p-c}^{\star}$ for $p \in \{a,b\}$ respectively are determined by the outer GFM control in per unit as

$$\frac{\mathrm{d}}{\mathrm{d}t}\delta_{a-c}^{\text{gfm}} = \omega_0 - k_P(\delta_{a-c}^{\text{gfm}} - \delta_{b-c}^{\text{gfm}}) + m_P(\Delta P_1), \tag{5a}$$

$$\tau\frac{\mathrm{d}}{\mathrm{d}t}V_{\delta,a-c}^{\text{gfm}} = -V_{\delta,a-c}^{\text{gfm}} - k_Q(V_{\delta,a-c}^{\text{gfm}} - V_{\delta,b-c}^{\text{gfm}}) + m_Q(\Delta Q_1), \tag{5b}$$

$$\frac{\mathrm{d}}{\mathrm{d}t}\delta_{b-c}^{\text{gfm}} = \omega_0 - k_P(\delta_{b-c}^{\text{gfm}} - \delta_{a-c}^{\text{gfm}}) + m_P(\Delta P_2), \tag{5c}$$

$$\tau\frac{\mathrm{d}}{\mathrm{d}t}V_{\delta,b-c}^{\text{gfm}} = -V_{\delta,b-c}^{\text{gfm}} - k_Q(V_{\delta,b-c}^{\text{gfm}} - V_{\delta,a-c}^{\text{gfm}}) + m_Q(\Delta Q_2). \tag{5d}$$

where $\Delta P_n := P_n^{\star} - P_n$ and $\Delta Q_n := Q_n^{\star} - Q_n$ for $n \in \{1,2\}$ are the deviations of the converter output powers from their setpoints $P_n^{\star}$ and $Q_n^{\star}$. Moreover, $k_P \in \mathbb{R}_{\geq 0}$ is the balancing feedback of $P-f$ droop, $k_Q \in \mathbb{R}_{\geq 0}$ is the balancing feedback of $Q-V$ droop. Then, the line-to-line GFM voltage reference is defined by $\angle v_{p-c,dq}^{\text{gfm}} = \theta_{p-c}^{\text{gfm}}$ and $\|v_{p-c,dq}^{\text{gfm}}\| = V_{p-c}^{\text{gfm}}$ for $p \in \{a,b\}$.

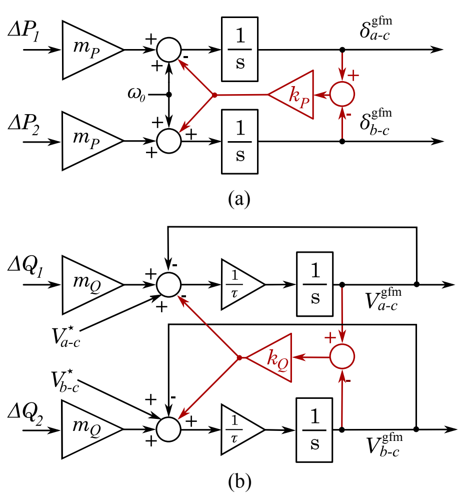

Fig. 3. $P-f$ (a) and $Q-V$ (b) droop control structure of generalized two-phase GFM control for three-wire connection. The balancing feedback (red) controls the difference between phase voltage magnitudes and phase angles.

The balancing of the two droop controllers in (5) through the balancing feedback with gain k_P and k_Q is shown in Fig. 3 (a) and Fig. 3 (b). Specifically, if k_P and k_Q are zero, the droop equations (4) reduce to two individual $P-f$ and $Q-V$ droop controls, which may result in three-phase unbalanced GFM reference voltages under unbalanced load. For instance, if $\Delta P_1 \neq \Delta P_2$, then the voltage phase angle differences may deviate from 120°. In contrast, if k_P and k_Q are increased, then the balancing feedback reduces the phase imbalance of the GFM reference voltage. Ultimately, as $k_P \to \infty$ and $k_Q \to \infty$, the voltage reference of two-phase GFM droop control in (5) converges to positive-sequence GFM droop control.

B. Dual-loop voltage and current control with current limiting

The reference voltage $v_{p-c,dq}^{\text{ref}}$ in dq-frame for $p \in \{a,b\}$ (e.g., generated by (5)) are tracked using dual-loop vector current and voltage proportional-integral (PI) controllers. To this end, for $p \in \{a,b\}$, the voltage PI controller $G_{\text{PI}}(s)$ is used to compute the filter current reference $i_{p,dq}^{\text{ref}} \in \mathbb{R}^2$, i.e.,

$$i_{p,dq}^{\text{ref}} = i_{o,p,dq} + Y_f v_{p-c,dq} + G_{\text{PI}}(s)(v_{p-c,dq}^{\text{ref}} - v_{p-c,dq}). \tag{6}$$

Here, $Y_f = \omega_0 R(\frac{\pi}{2})c_f$ denotes the filter admittance matrix, $v_{p-c,dq}^{\text{ref}}$ denotes the voltage reference, and $i_{o,p,dq} \in \mathbb{R}^2$ denotes the output current of the converter. Next, $i_{p,dq}^{\text{ref}}$ is passed to inner current PI loop which is implemented for $p \in \{a,b\}$ as

$$v_{\text{sw},p-c,dq} = v_{p-c,dq} + Z_f i_{p,dq} + G_{\text{PI}}(s)(\rho_p^{\text{lim}} i_{p,dq}^{\text{ref}} - i_{p,dq}), \tag{7}$$

where $Z_f = r_f\mathbb{I}_2 + \omega_0 R(\frac{\pi}{2})l_f$ denotes the filter impedance matrix ($\mathbb{I}_2$ is 2×2 identity matrix), $v_{\text{sw},p-c,dq} \in \mathbb{R}^2$ is the line-to-line switching voltage modulated by the VSC, $i_{p,dq} \in \mathbb{R}^2$ is the filter current of the converter, and $\rho_p^{\text{lim}} \in \mathbb{R}_{>0}$ is a multiplier used for current limiting. From $v_{\text{sw},a-c,dq}$ and $v_{\text{sw},b-c,dq}$ we obtain their respective time domain signals $v_{\text{sw},a-c}(t)$ and $v_{\text{sw},b-c}(t)$ by transforming from their respective rotating dq frame to stationary frame using $\theta_{a-c}^{\text{gfm}}$ and $\theta_{b-c}^{\text{gfm}}$ from (5). Then, the line-to-line switching voltages are computed by,

$$v_{\text{sw},a-b}(t) = v_{\text{sw},a-c}(t) - v_{\text{sw},b-c}(t). \tag{8}$$

We pass all three line-to-line to voltages to a delta-star transformation (assuming floating neutral) to obtain $v_{\text{sw},a}(t)$, $v_{\text{sw},b}(t)$ and $v_{\text{sw},c}(t)$ which are used to compute gate signals using standard pulse-width modulation algorithms.

Using the above controls, current limiting of $i_{p,dq}^{\text{ref}}$ to the maximum current $I_{\max}$ can either be implemented through (i) the well-known current saturation algorithm (CSA) and multiplier ρ_p^{lim} (see Sec. IV-C) or, (ii) by modifying the voltage reference $v_{p-c,dq}^{\text{ref}}$ through threshold virtual impedance (TVI) [13] (see Sec. IV-D).

C. Unbalanced CSA for three-wire connection

The voltage reference with CSA is given by $v_{p-c,dq}^{\text{ref}} = v_{p-c,dq}^{\text{gfm}}$ and CSA limits $i_{p,dq}^{\text{ref}}$ for $p \in \{a,b\}$ as

$$i_{p,dq}^{\text{lim}} := \rho_p^{\text{ref}} i_{p,dq}^{\text{ref}}, \tag{9}$$

where $\rho_p^{\text{ref}} := \min(1, \frac{I_{\max}}{\|i_{p,dq}^{\text{ref}}\|})$ and $I_{\max} \in \mathbb{R}_{>0}$ is the maximum phase current magnitude. In other words, ρ_p^{ref} is used to limit the filter currents i_a and i_b when using the CSA. To implement CSA for i_c we need to control $i_{a,dq}^{\text{lim}}$ and $i_{b,dq}^{\text{lim}}$. The filter current $i_c(t)$ can be obtained from $i_c(t) = -i_a(t) - i_b(t)$ where $i_a(t), i_b(t), i_c(t) \in \mathbb{R}$ are instantaneous filter current measurements. Recall that the filter current reference $i_{p,dq}^{\text{ref}}$ computed from (6) is in dq frame with respect to $\theta_{p-c}^{\text{gfm}}$, i.e,

979-8-3315-8138-1

$i^{\text{ref}}_{a,dq} = R(\theta^{\text{gfm}}_{a-c})[i^{\text{ref}}_a, i^{\text{ref},\perp}_a]^\mathsf{T}$ and $i^{\text{ref}}_{b,dq} = R(\theta^{\text{gfm}}_{b-c})[i^{\text{ref}}_b, i^{\text{ref},\perp}_b]^\mathsf{T}$, where filter reference current i^{ref}_p and $i^{\text{ref},\perp}_p$ are stationary frame α and β components respectively, discussed in Sec. III for $p \in \{a, b\}$. This is also illustrated in the Fig. 2 (b) where the d axis phasor of $i^{\text{ref}}_{a,dq}$ and $i^{\text{ref}}_{b,dq}$ is aligned to the v_{a-c} and the v_{b-c} phasors respectively. Therefore, we first transform $i^{\text{ref}}_{b,dq}$ to the frame of $i^{\text{ref}}_{a,dq}$ and then obtain $i^{\text{ref}}_{c,dq}$ as

$$i^{\text{ref}}_{c,dq} = -i^{\text{ref}}_{a,dq} - R(\theta^{\text{gfm}}_{b-c} - \theta^{\text{gfm}}_{a-c})[i^{\text{ref}}_{b,d}, i^{\text{ref}}_{b,q}]^\mathsf{T}. \tag{10}$$

Here, $i^{\text{ref}}_{c,dq}$ is in a dq frame rotating with the frequency ω_{a-c}. When $\|i^{\text{ref}}_{c,dq}\| > I_{\max}$, then, because $i^{\text{ref}}_{c,dq}$ is not directly controllable, $i^{\text{lim}}_{p,dq}$ for $p \in \{a, b\}$ needs to be modified to limit $i^{\text{ref}}_{c,dq}$. To this end, we define limiting multiplier

$$\rho^{\text{lim}}_p := \rho^{\text{ref}}_c \rho^{\text{ref}}_p \tag{11}$$

for $p \in \{a, b\}$. Notably, the multiplier $\rho^{\text{ref}}_c := \min(1, \frac{I_{\max}}{\|i^{\text{ref}}_{c,dq}\|})$ has a similar interpretation to ρ^{ref}_a and ρ^{ref}_b.

To avoid harmonic injections, the CSA implemented in (9) and (11) does not clip the current waveform but instead adjusts the magnitude of the reference current. Moreover, the angle of the reference current is preserved.

D. Unbalanced TVI for three-wire connection

Another well-known current limiting method, which results in reduced transients during post-fault recovery, is threshold virtual impedance (TVI). When TVI is used instead of CSA, it holds that $\rho^{\text{lim}}_p = 1$ for $p \in \{a, b\}$. Instead, the voltage drop

$$v_{p,dq,\text{TVI}} = \begin{bmatrix} R_{p,\text{TVI}} & X_{p,\text{TVI}} \\ -X_{p,\text{TVI}} & R_{p,\text{TVI}} \end{bmatrix} \begin{bmatrix} i^{\text{ref}}_{p,d} \\ i^{\text{ref}}_{p,q} \end{bmatrix}. \tag{12}$$

over a virtual impedance with resistance $R_{p,\text{TVI}}$ and reactance $X_{p,\text{TVI}}$ for each phase $p \in \{a, b, c\}$ is used for current limiting. To implement the unbalanced TVI (12) for a three-wire connection, (12) is used to compute the line-to-neutral voltage drop over the TVI which is subsequently converted to line-to-line voltage drops that are subtracted from the GFM reference voltages to obtain $v^{\text{ref}}_{p-c,dq}$ in dq-frame for $p \in \{a, b\}$.

To this end, given the filter current reference magnitude $\|i^{\text{ref}}_{p,dq}\|$ we define the virtual resistance $R_{p,\text{TVI}} = \max(0, k_{TVI}\|i^{\text{ref}}_{p,dq}\| - I_{\text{th}})$ with TVI gain $k_{TVI} \in \mathbb{R}_{>0}$ and threshold $I_{\text{th}} \in \mathbb{R}$. Moreover, the virtual reactance is given by the TVI reactance-to-resistance ratio $X_{\text{TVI}}/R_{\text{TVI}}$ and $X_{p,\text{TVI}} = X_{\text{TVI}}/R_{\text{TVI}} R_{p,\text{TVI}}$. In other words, the virtual impedance increases if the filter current magnitude exceeds the threshold I_{th}. We first obtain $i^{\text{ref}}_{c,dq}$ from to (10), then we calculate the TVI-induced line-to-neutral voltage drop $v_{p,dq,\text{TVI}}$ per phase as (12). We then convert this line-to-neutral TVI voltage drop $v_{p,dq,\text{TVI}}$ into a line-to-line voltage drop. To this end, recall that $i^{\text{ref}}_{c,dq}$ is already aligned with the v_{a-c} phasor, hence $v_{c,dq,\text{TVI}}$ is also aligned with the v_{a-c} phasor. Moreover, we change the frame of $v_{c,dq,\text{TVI}}$ in (13b) from the v_{a-c} phasor to the v_{b-c} phasor before calculating $v_{b-c,dq,\text{TVI}}$. Thus, the TVI-induced line-to-line voltage drop is given by

$$v_{a-c,dq,\text{TVI}} = v_{a,dq,\text{TVI}} - v_{c,dq,\text{TVI}}, \tag{13a}$$

$$v_{b-c,dq,\text{TVI}} = v_{b,dq,\text{TVI}} - \mathcal{R}(\theta^{\text{gfm}}_{a-c} - \theta^{\text{gfm}}_{b-c}) \begin{bmatrix} v_{c,d,\text{TVI}} \\ v_{c,q,\text{TVI}} \end{bmatrix}. \tag{13b}$$

Finally, we assign the voltage reference in (6) as

$$v^{\text{ref}}_{p-c,dq} = v^{\text{gfm}}_{p-c,dq} - v_{p-c,dq,\text{TVI}}. \tag{14}$$

V. Case Study

We use an EMT simulation of a switching model of a two-level dc/ac VSC with delta-connected filter capacitors and floating dc bus, connected to a transmission system modeled as a double-circuit transmission line and infinite bus. The system and parameters are shown in Fig. 4. The VSC is connected to a 1 km medium voltage feeder through a transformer and the (closed) breaker S_1. The medium voltage feeder connects to a 40 km double-circuit high voltage transmission line through a step-up transformer. The generalized two-phase GFM control ($m_P = m_Q = 5\%$) is implemented at a sampling rate of 10 kHz. The switching frequency of the VSC is also set at 10 kHz.

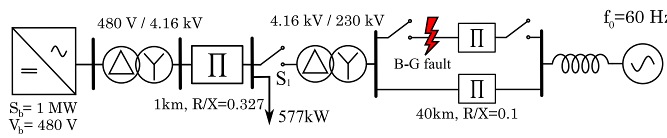

Fig. 4. Test system with a low-voltage VSC connected to a weak ac system through step-up transformers, a medium-voltage feeder, and a double-circuit transmission line.

Initially, the system is in a balanced steady state and the power setpoints $P^\star_1 = P^\star_2 = 0.45$ p.u. result in a total active power output of the GFM converter of $P^\star_1 + P^\star_2 = 0.9$ per unit. To demonstrate the proposed GFM control ability to limit current during fault, we simulate a single-line-to-ground fault (phase b to ground) at $t = 3$s that is cleared after ten cycles at 60 Hz. Note that, before the fault, the system is balanced and hence all phase quantities are identical. Line-to-line voltage magnitudes are shown in Fig. 5, while the currents, active powers, and reactive powers shown in Fig. 5 are phase filter currents and powers. The current and the voltage magnitudes shown in Fig. 5 are computed using the maximum value in each ac cycle to avoid artifacts introduced by, e.g., the Hilbert transform (1). In contrast, the active and reactive powers shown are filtered estimates for the phase powers obtained by applying a Fourier Transform to extract their 60 Hz components, i.e., remove double frequency components.

The response obtained using CSA is shown in the left column of Fig. 5 while results obtained with TVI are shown in the right column. Using CSA, the current of phase c immediately reaches $I_{\max} = 1.2$ p.u. after fault inception and the magnitude of v_{b-c} significantly drops once the current limit has been reached. The TVI threshold has been selected as $I_{\text{th}} = 1.1$ p.u., $X_{\text{TVI}}/R_{\text{TVI}} = 1$ for all $p \in \{a, b, c\}$ and $k_{\text{TVI}} = 4.4$. Due to the proportional response of the TVI, the current of phase c is limited at approximately 1.1 p.u. (i.e., less than $I_{\max} = 1.2$ p.u.).

Once the fault is cleared after ten ac cycles at $t = 3.166s$ by disconnecting the affected line segment, Fig. 5 shows resynchronization transients in the GFM converter response. Using CSA, the converter exhibits significant resynchronization transients for voltage, active power, and reactive power. Moreover, the settling time to the post-fault equilibrium is

979-8-3315-8138-1

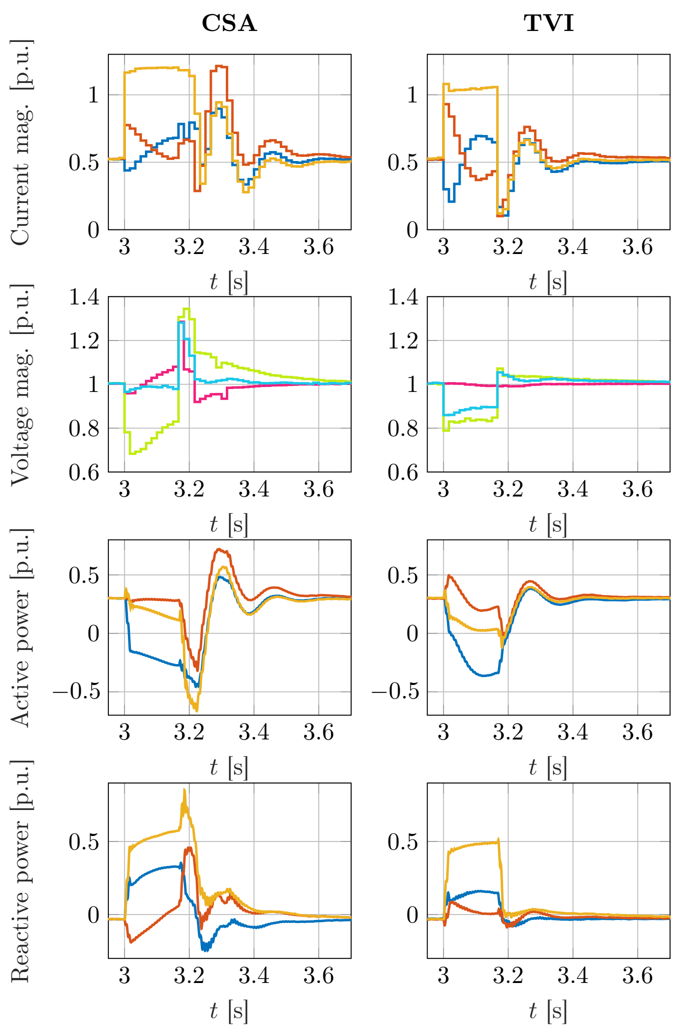

Fig. 5. Response of GFM converter to a phase b to ground fault on a transmission line between $t = 3$ s and $t = 3.166$ s. Voltage magnitudes are shown for line-to-line voltages v_{a-b} (—), v_{b-c} (—), v_{c-a} (—). Current magnitudes and estimated instantaneous powers are shown for phase a (—), b (—), c (—). The base values are $S_b = 1$ MW and $V_b = 480$ V (see Fig. 4).

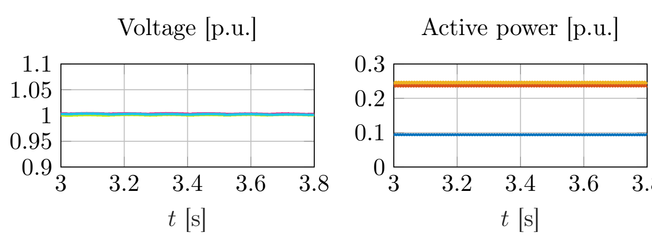

Fig. 6. Response of GFM converter supplying an unbalanced 577 kW load while islanded. The plot colors and base values are identical to Fig. 5

significant. In contrast, when TVI is used, the settling time is shorter and the transients are significantly reduced, which can be attributed to the TVI reducing integrator wind-up in the voltage loop. Nevertheless, using TVI, the GFM converter can inject 91% of its maximum current $I_{\max}$. Additionally, we also test the stand-alone capability of the GFM converter by connecting 580 kW of highly unbalanced linear load and opening breaker S_1. In this case, the converter is able to supply the load while maintaining balanced line-to-line voltages as shown in Fig. 6.

VI. Conclusion

This paper considered GFM control for three-phase dc/ac voltage source converters with three-wire connection. To this end, this work proposed a GFM droop control that combines individual GFM controls for two controllable phases with a phase balancing feedback. Moreover, the voltage references generated by the generalized two-phase outer GFM control are tracked by inner dual-loop current and voltage controls for each phase that enable direct limiting of phase currents without clipping of current waveforms. In contrast to previous works in literature, this approach maintains full control of the VSC terminal voltage and enables effective limiting of phase currents through current saturation and virtual impedance during unbalanced faults. A high-fidelity case study is used to demonstrate the effectiveness of the proposed control under unbalanced medium-voltage loads and unbalanced faults.

References

[1] W. E. Gnibga, A. Blavette, and A.-C. Orgerie, "Renewable energy in data centers: The dilemma of electrical grid dependency and autonomy costs," *IEEE Transactions on Sustainable Computing*, vol. 9, no. 3, pp. 315–328, 2024.

[2] J. Rocabert, A. Luna, F. Blaabjerg, and P. Rodríguez, "Control of power converters in AC microgrids," *IEEE Trans. Power Electron.*, vol. 27, no. 11, pp. 4734–4749, 2012.

[3] M. Yao, I. A. Hiskens, and J. L. Mathieu, "Mitigating voltage unbalance using distributed solar photovoltaic inverters," *IEEE Trans. Power Syst.*, vol. 36, no. 3, pp. 2642–2651, 2021.

[4] D. Groß, M. Colombino, J.-S. Brouillon, and F. Dörfler, "The effect of transmission-line dynamics on grid-forming dispatchable virtual oscillator control," *IEEE Trans. Control Netw. Syst.*, vol. 6, no. 3, pp. 1148–1160, 2019.

[5] M. A. Awal, M. R. K. Rachi, H. Yu, I. Husain, and S. Lukic, "Double synchronous unified virtual oscillator control for asymmetrical fault ride-through in grid-forming voltage source converters," *IEEE Trans. Power Electron.*, 2022.

[6] P. Bhagwat and D. Groß, "Three-phase grid-forming droop control for unbalanced systems and fault ride through," in *IEEE Power & Energy Society General Meeting*, 2023.

[7] B. Majmunović, T. Dragičević, and F. Blaabjerg, "Multi objective modulated model predictive control of stand-alone voltage source converters," *IEEE Journal of Emerging and Selected Topics in Power Electronics*, vol. 8, no. 3, pp. 2559–2571, 2020.

[8] P. Lakshmanan, P. Janakiraman, S. K. Ram, and A. Abhishek, "Fpga-based digital control implementation of unbalance compensation in three-phase three-wire stand-alone inverters," in *IEEE Power India International Conference*, 2022.

[9] J. He, X. Zhang, H. Ma, and C. Cai, "Lyapunov-based large-signal control of three-phase stand-alone inverters with inherent dual control loops and load disturbance adaptivity," *IEEE Trans. Ind. Electron.*, vol. 68, no. 9, pp. 8391–8401, 2021.

[10] S. Lee, K.-j. Lee, and D.-s. Hyun, "Modeling and control of a grid connected VSI using a delta connected LCL filter," in *Annual Conference of IEEE Industrial Electronics*, 2008, pp. 833–838.

[11] H. W. Beaty and D. G. Fink, *Handbook of Electric Power Calculations*, 4th ed. McGraw-Hill Education, 2015.

[12] T. Kim, N. G. Barry, W. Kim, S. Santoso, W. Wang, R. C. Dugan, and D. Ramasubramanian, "Voltage balancing capability of grid-forming inverters," *IEEE Open Access Journal of Power and Energy*, vol. 9, pp. 479–488, 2022.

[13] A. D. Paquette and D. M. Divan, "Virtual impedance current limiting for inverters in microgrids with synchronous generators," *IEEE Trans. Ind. Appl.*, vol. 51, no. 2, pp. 1630–1638, 2015.

979-8-3315-8138-1